JKAU: Sci., **Vol. 34**, No. 1, pp: 85 - 105 (2024)
DOI:10.4197/Sci.34-1.6

Simplified Approach for Environmental Remediation of Methylene Blue and Crystal Violet from Aqueous Solution Utilizing Nanoclay Material: Kinetic, Isotherm, Thermodynamic Studies

Mohamed A. Abdel-Fadeel

Chemistry Department, Faculty of Science, King Abdulaziz University, Jeddah 21589, Saudi Arabia, and Biomedical Laboratory, Chest Hospital, Mansoura, Dakahlia, Egypt

m_abdelazeem@hotmail.com

Abstract. This paper explains a rapid, simple, easy, and eco-friendly method for the elimination of the dyes Crystal Violet (CV) and Methylene Blue (MB) from aquatic solutions onto the eco-friendly Halloysite Nanoclay (HSNC) solid phase. Physical features of the HSNC, such as SEM, TEM, XRD, FTIR, and BET, were studied. The study examined various parameters that impacted adsorption efficiency, including pH solution, adsorbent dosage, temperature, shaking time, and KNO_3 concentration. The efficiency of CV and MB dyes' adsorption on HSNC was studied kinetically, and the obtained data showed the processes were organized via a pseudo-second order (PSO) system. The calculated adsorption capacity (qe,cal) was 46.72 mg/g for CV and 43.46 mg/g for MB dyes on HSNC. Under the best conditions, the Langmuir model was found to be suitable for explaining the isotherm behavior for removing dyes by HSNC, with a maximum adsorption capacity (qm) of 45.25 mg/g for CV and 44.44 mg/g for MB. Also, the thermodynamic study indicates the removal of CV and MB dyes is an endothermic process, and the adsorption of dyes is a chemisorption and spontaneous process. Finally, testing the elimination efficiency of CV and MB dyes based on three different actual samples on HSNC gave (E%) more than 93%. Overall, it was discovered that HSNC was an inexpensive, ecologically friendly substance for eliminating cationic CV and MB dyes.

Keywords: Crystal Violet, Methylene Blue, Nanoclay, Removal, kinetics, Isotherm, Thermodynamic.

1. Introduction

The pollution of water is a major worldwide issue, mostly caused by various industrial effluents, comprehensive those from the food, paint, printing, pharmaceutical, and textile industries. Hazardous contaminants found in these industrial waste streams have historically led to several health and environmental issues. These inorganic contaminants' tendency to accumulate in living things is the cause of their ubiquitous prevalence in groundwater [1]. Because of their chemical stability and versatility, azo dyes make up more than 50% of all dyes used in everyday applications [2]. However, azo dyes' great economic dependency raises serious concerns about their toxicity, carcinogenicity, and lack of biodegradability. Despite being widely used in business; cationic dyes are more dangerous than other types. Environmental contamination results from the estimated 12% of yearly cationic dye production that is dumped in industrial water streams [3]. The majority of these colors are harmful, non-biodegradable, teratogenic, and carcinogenic; they can cause allergic dermatitis and mutations. Moreover, it poses major risks to ecosystems and human health [4]. However, the inability of the treatment methods to fully degrade and mineralize the dyes renders them insufficient. Therefore, removing these pollutants

from water bodies is essential to maintaining a clean and safe environment. While there are several ways to get rid of dyes in aquatic environments, oxidation, photodegradation, electrochemical treatment, coagulation, ozonation, flocculation, biological degradation, and adsorption are some of the most common techniques [5–9]. Adsorption is one of the numerous chemical and physical techniques that have been successfully applied to remove colors from wastewater [10, 11]. A novel class of solid-phase adsorbents known as Nano-adsorbents is being effectively employed to remove different pollutants from contaminated aquatic solutions. Single-walled carbon nanotubes, nanoclay, multi-walled carbon nanotubes, nanographene, and their composites are some examples of Nano-adsorbents for removing/adsorbing different pollutants (such as heavy metals and organic compounds) from aqueous environmental solutions [12–21]. For the long-term release of active agents, a natural mineral that is both affordable and biocompatible is Halloysite nanoclay (HSNC). High surface area, biocompatibility, and the capacity to interact with pollutant molecules through ion exchanger action or surface adsorption are just a few of the special qualities that HSNC has to offer [18]. A double layer of silicon, aluminum, oxygen, and hydrogen makes up the unique and multifunctional nanomaterials known as Halloysite, which were naturally produced over millions of years on the earth.

This study aims to use HSNC as a solid phase to adsorb/remove cationic dyes such as methylene blue and crystal violet with high efficiency from the aqueous environment. This work studied the physical characterization of HSNC and the optimum conditions to obtain the best removal/adsorption efficiency. Kinetic models and thermodynamic parameters were calculated to determine the removal mechanism for this process. Lastly, the efficiency of this method was tested for the adsorption of dyes from three different water samples.

2. Experimental

2.1. Materials

I purchased Halloysite Nanoclay (HSNC), Crystal Violet dye (CV), and Methylene Blue (MB) dye through "Sigma Aldrich" in the United States. Additionally, every chemical used is of analytical purity and suitable for reagents. Each dye was produced as a stock solution (1000 mg/L) by dissolving 0.1 gram of each dye in 100 ml of deionized water. The dilution law was used to create additional diluted solutions of dye (5–50 mg/L). In the adsorption process of dyes by the HSNC solid phase, a series of HCl and/or NaOH (0.2mol/L) solutions of pH (2-11) were utilized as an extracting medium.

2.2. Characterization Techniques and Instrument

I looked at the physical properties of HSNC using a scanning electron microscope (SEM), an X-ray diffraction (XRD) pattern, an FT-IR spectrum, a transmission electron microscope (TEM), and the specific surface area (BET). Every spectrophotometric measurement was recorded using a UV-visible (Perkin-Elmer) instrument. More details about this section are in my previous research [22].

2.3. Adsorption Experiment

In two (250 ml) conical flasks, an exact amount (0.010 ± 0.0002 g) of the HSNC solid phase was equilibrated with 75 ml of the solution of each dye (CV and MB), including a 7.5

mg/L concentration at pH 9 for CV and pH 8 for MB at room temperature. For 120 minutes, the examined solution was automatically shaken. After equilibrium, the aquatic solution was separated, and the amount of dyes that remained was determined using a UV–Vis spectrophotometer. This was done by determining each dye's absorbance in the aquatic solution both before and after adsorption, at a wavelength of 590 nm for CV dye and 664 nm for MB dye [23]. Lastly, equation (1) expresses the percentage of separation efficiency (%E). Then the amount of dyes adsorbed (q_t) on HSNC expressive was calculated using formula (2).

$$\% E = \frac{C_o - C_t}{Co} x\ 100 \quad (1)$$

$$q_t = \frac{(C_o - C_t)\, V}{m} \quad (2)$$

In which C_o is the original conc. of dye and C_t is the remaining conc. of dye after shaking.

2.4. Collection of Real Water Samples

The efficiency of solid-phase HSNC sorbent in the extraction and recovery of CV and MB dyes from Red Sea water, wastewater, and tap water was examined. The samples were collected from the Red Sea in Jeddah, Saudi Arabia, the King Abdulaziz University's Membrane Bioreactor Technology Wastewater, and the Chemistry Department's lab at the same university, in that order. The samples were placed in Teflon bottles and maintained at 5 ^{o}C in the dark after being passed through filters using a 0.45 m membrane. Samples of 75 milliliters were adjusted to pH 9 for CV dye and pH 8 for MB using NaOH (0.2 mol/L) and shaken together with the HSNC adsorbent. The dye concentrations that were returned were finally calculated using spectrophotometry.

3. Results and Discussions

The HSNC solid phase was used to remove methylene blue and crystal violet as cationic dyes with high efficiency from the aqueous environment. Fig. 1. Recording of electronic bands of CV (7.5 mg/L) dye and MB (7.5 mg/L) dye in the aquatic phase revealed absorption sharp peaks at 590 nm aimed at CV [Fig. 1a] and 664 nm for MB (Fig. 2a). However, these peaks decreased significantly after shaking CV (Fig. 1b) and MB (Fig. 2b) dyes with 10 mg of the HSNC solid phase. This behavior validates the HSNC solid phase's ability to effectively remove dyes from the aquatic phase.

3.1. Characterization of HSNC Solid Phase

In order to examine the physical properties of HSNC: SEM, FTIR, XRD, TEM, and BET were applied. HNC consists of a hollow tubular structure measuring approximately 1 μm in length and 60 nm in diameter, as the TEM and SEM images (illustrated in Fig. 2, 3) unequivocally demonstrate. The cross-aggregations that result from static electric charges between the nanotubes are also visible in the images [24]. The peaks of reflection at scattering angles 2θ = 11.81°, 19.89°, 24.58°, 35.03°, 36.71°, and 38.09°, that relate to the reflecting planes (001), (110), (002), (122), (200), and (131) diffraction planes are explained by the XRD spectrum of HNC in Fig. 4 [25]. For the HSNC, an initial gap (001) of 7.49 Å (2θ =11.81°) was found. The FTIR analysis provides an explanation for the virgin HSNC functional groups on the surface. The stretching vibrations of the hydroxyl group (OH) of the Al-OH groups on the outer and inner

surfaces, respectively, are detected by the bands at 3696 cm^{-1} and 3623 cm^{-1}, as shown in Fig. 5. The characteristic bands of stretch of O-H of inserted water, O-H deformation of water, and Si–O vibration widening bands were found at 3445 cm^{-1}, 1651 cm^{-1}, and 1035 cm^{-1}, respectively. The bands observed at 794 and 754 cm^{-1} are indicative of O-H translation vibrations occurring within the HSNC (O-H) units. The spectra of HNT2-HNT5 samples exhibited variability, which is further corroborated by the bands spanning from 600 to 1750 cm^{-1}. The bands seen at 794 and 911 cm^{-1} represent the distinctive peaks of kaolinite. The bands seen between 2800-2900 cm^{-1} [26] suggest the presence of acrylate, an organic compound often employed in clay production. In Fig. 6, the N_2 adsorption/desorption isotherms pertaining to HSNC were categorized as type III isotherms; furthermore, the BET was determined to be 72.8 m^2/g.

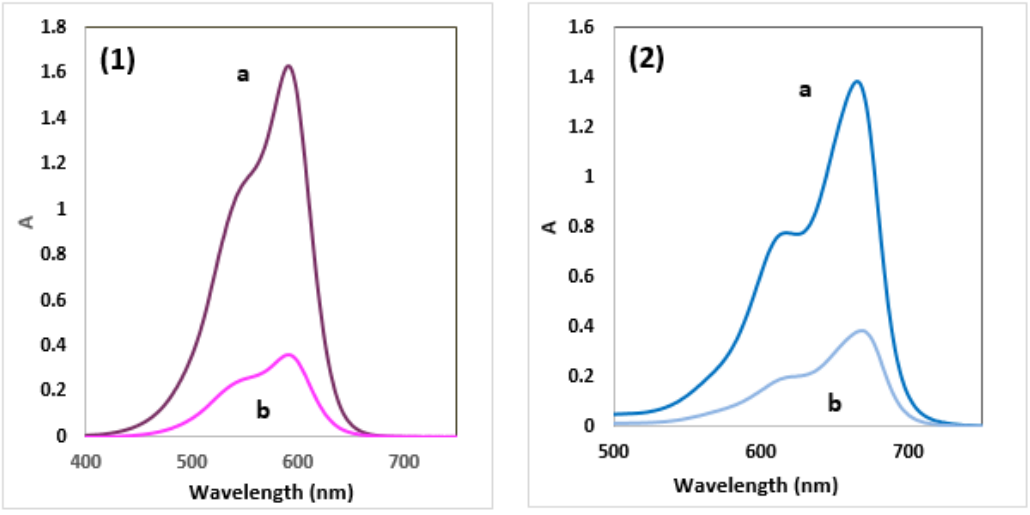

Fig. 1. The spectra of UV-Vis of CV dye (7.5 ppm) in solution devoid of HSNC (1a) following a shake with 10 mg of HSNC (1b). Additionally, the MB dye (5 ppm) spectrum in a solution absent of HSNC (2a) when shaking with 10 mg of HSNC (2b).

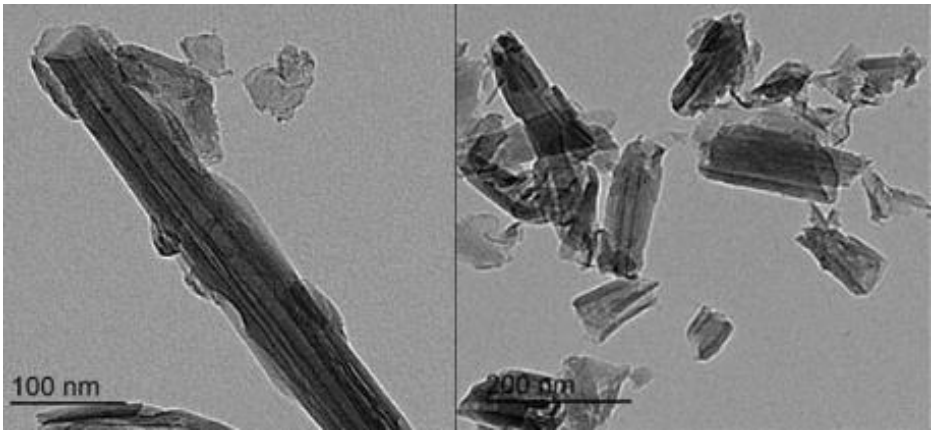

Fig. 2. Images of TEM for HSNC.

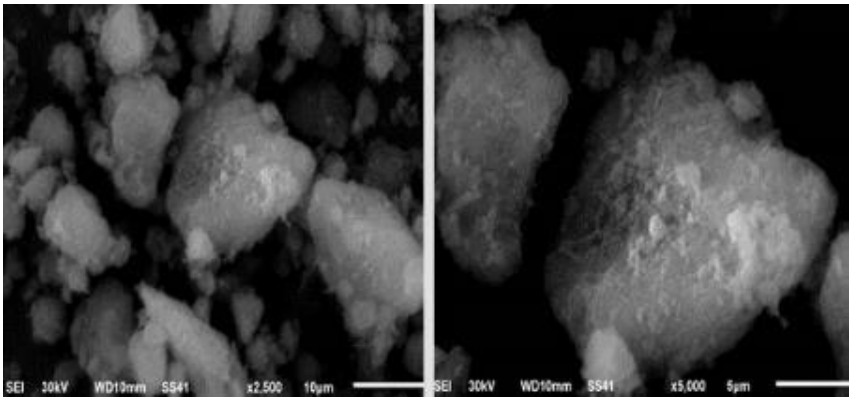

Fig. 3. Images of SEM for HSNC.

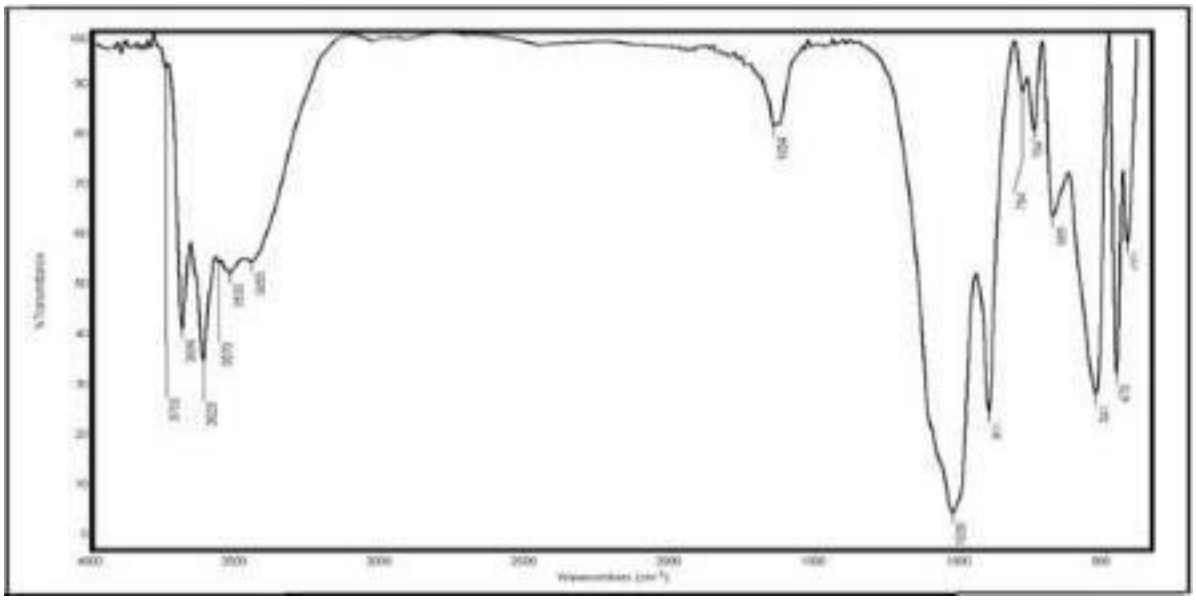

Fig. 4. The FTIR of HSNC.

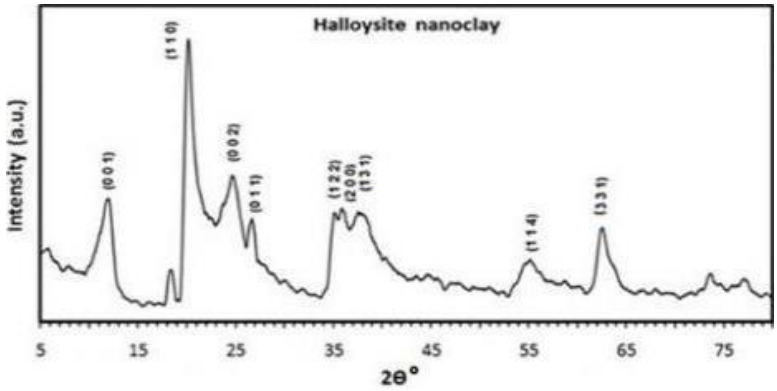

Fig. 5. The pattern of XRD for HSNC

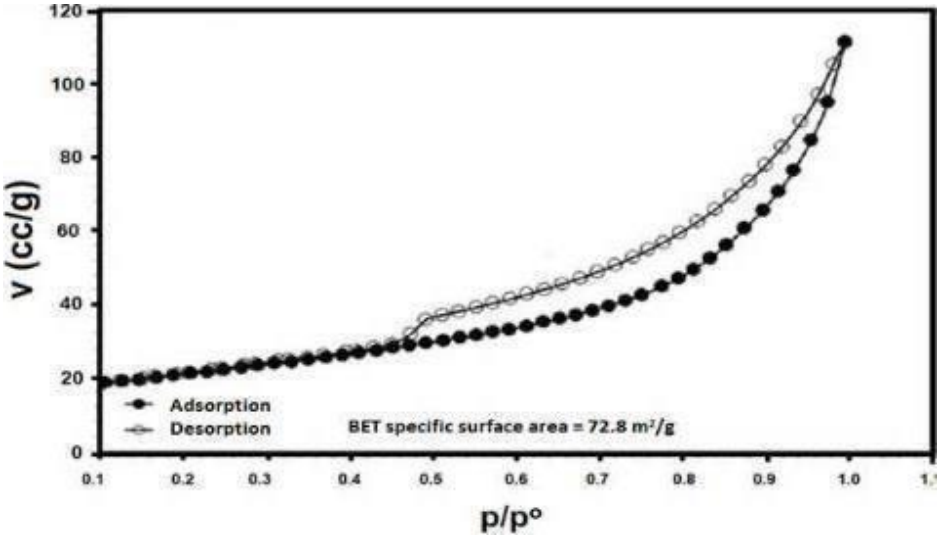

Fig. 6. Curve of BET for HSNC at 77K.

3.2. Adsorption Investigation

The pH of the solution is one of the important factors in the adsorption process of dyes and heavy metals. To determine how the solution's pH level affected the adsorption of CV and MB dyes onto HSNC at high pH (2:10) levels using a NaOH/HCl mixture and at room temperature for 120 min. The results presented in (Fig. 7) showed that the protonation process in the active locations with many protons [H^+] enhanced the extraction efficiency of dye agents as pH rose. These protons vie with cationic compound dyes (CV and MB) for available sites of activity. In alkaline solutions, the amount of -ve charges on CV and MB dyes were increased, and the active sites were completely ionized, and this led to a raise in the removal efficiency, as shown in (Fig. 7) [27]. Therefore, the ideal values of pH solution were chosen as 9 and 8 for CV and MB dyes, respectively, which were adjusted by NaOH (0.1 mol/L).

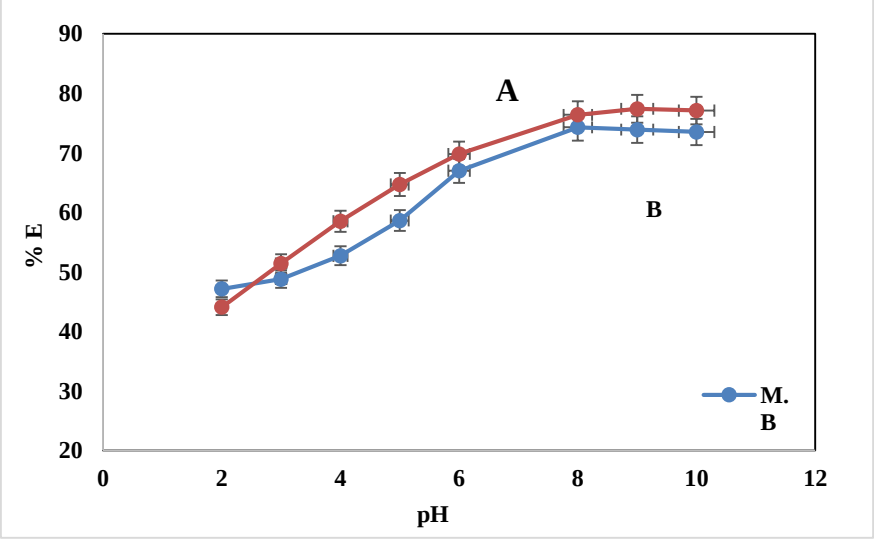

Fig. 7. Influence of pH solution on adsorption percentage of CV (A) and MB (B) dyes in aquatic solution were tested on 0.010 ± 0.0002 g of HSNC solid phase.

For CV and MB dyes, the impact of HSNC bulk on dye efficiency in adsorption was investigated using a dosage of 7.5 mg/L (Fig. 8). The graph displayed that as the HSNC solid phase quantity was raised to 25 mg from 2.5 mg, the effectiveness of the removal increased from 38.5% to 99.7% for CV and from 33.4% to 99.1% for MB dye. This effect is attributed to the existence of more sites for adsorption because of the mass increase and the rise in the HSNC surface area. In this work, 10 mg of mass from the HSNC solid phase was used for the removal of CV and MB dyes, which corresponded to 77.6% and 72.9%, respectively, for the removal process to be enabled to see how other factors affect the adsorption process.

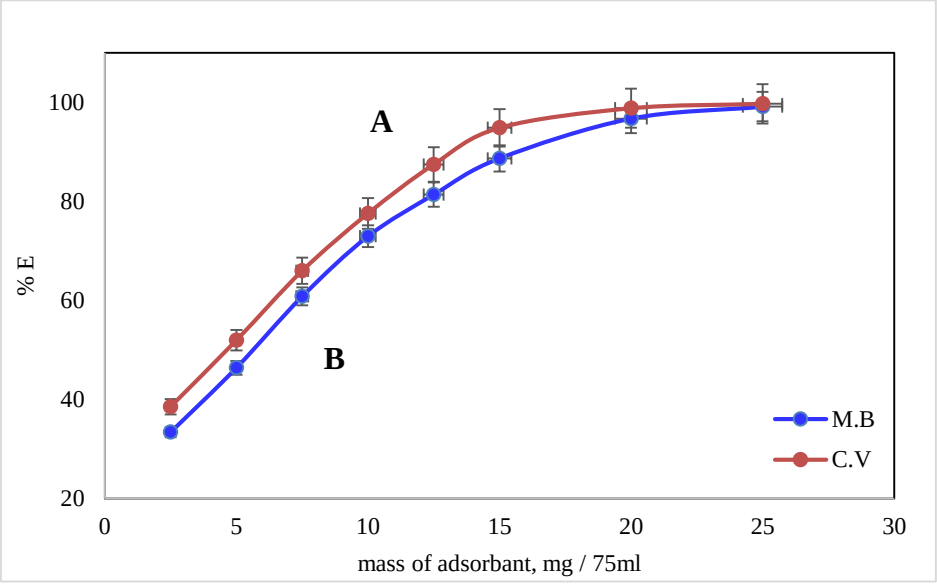

Fig. 8. Impact of HSNC solid phase mass on elimination efficiency of CV (A) and MB (B) dyes (7.5 ppm) with a shaking time of 120 min and at 22 ± 0.5 ºC.

In dye adsorption investigations, contact time is one of the most important characteristics. Figure 9 explains the influence of adsorption of CV also MB dyes via HSNC duration. The figure illustrates that the adsorption efficiency increases rapidly during the first 60 minutes. This result may be Attributed to transfer dye species form the solution to the outer surface of HSNC, which has a large number of active sites available and suitable for adsorbed dyes species. The removal efficiency reached equilibrium within 90 minutes, which the slow process was due to the dye species' diffusion within the HSNC packages.

At constant shaking time, the influence of temperature solutions on the removal efficiency of dyes by HSNC was studied at different four degrees (10, 22, 35, and 50 ºC). Data indicated that increasing the solution's temperature increased the CV and MB dyes extraction rate onto HSNC (Fig. 10), a behavior that supports the endothermic character of the adsorption process.

The effect of potassium nitrate (KNO_3) concentrations as ionic strength on the exclusion percentages of dyes species is essential due to It can create various adsorption modes by means of the electrostatic attraction between each type of dyes and the HSNC surfaces. The results data in (Table 1) show a small drop in the percentages of dyes removed when the amounts of KNO_3 in the mixture grow. Due to the charge level at the adsorption solid phase, the occurrence

of a cation, such as K^+, prevents the association of dye molecules with the adsorbed solid-state surface [28].

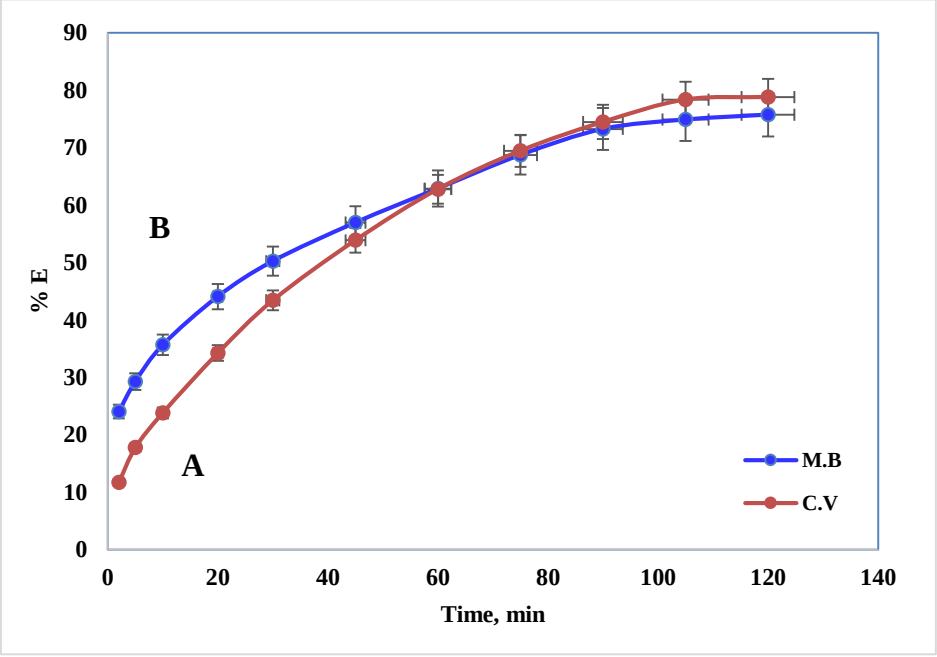

Fig. 9. Impact of contact duration on removal efficiency of CV (A) and MB (B) dyes (7.5 ppm) at pH 9 and 8 respectively, by (0.010 ± 0.0002 g) of HSNC at 22 ± 0.5 ºC.

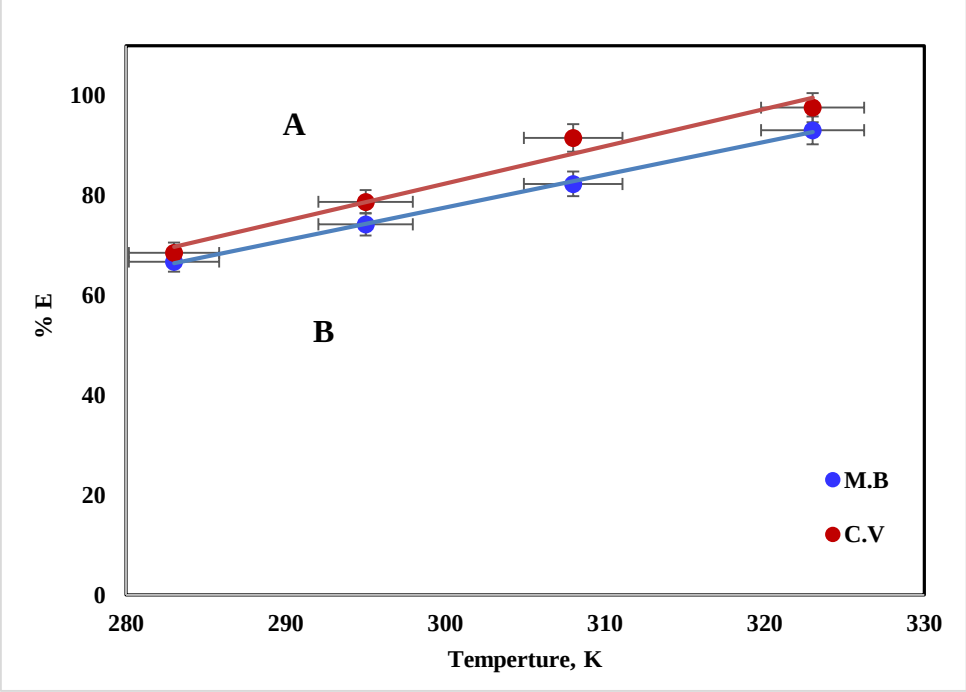

Fig. 10. Impact of temp. on the removal effectiveness of CV (A) and MB (B) dyes (7.5 ppm) at pH 9 and 8 respectively, by (0.010 ± 0.0002 g) of HSNC solid phase with shaking for 120 min.

Table 1. Influence of KNO_3 concentration on removal effectiveness of dyes (CV and MB).

KNO_3 Conc. (M)	C.V (% E)	M.B (% E)
0	78.408	73.080
0.02	77.129	70.860
0.04	76.127	68.640
0.06	74.903	66.883
0.08	73.957	65.032

3.3. Diffusion Models Study

The amount of dyes retained on the HNC adsorbing surface is influenced by the gross rate of transport, intraparticle diffusion, and film diffusion; the faster one regulates the gross rate of transport, which in turn impacts the amount of dyes retained on the HNC solid phase. The Weber and Morris model of intraparticle diffusion (IPD) for CV and MB dyes removal by HSNC is derived as follows [29]:

$$q_t = K_{id}(t)^{1/2} + C \quad (3)$$

In which the capacity of the adsorption at any given time (t) is denoted by q_t, K_{id} is the rate of diffusion within particles. (mg/g $min^{1/2}$), plus a constant percentage of the border layer's thickness is C (mg/g).

Using the model of intraparticle diffusion (IPD), every experimental adsorption result with a zero intercept has good straight lines pass via the origin using the correlation coefficient (R^2) 0.9935 in the case of CV dye (Fig. 11), which confirms that the IPD model is suitable for all experimental results. But for M.B dye bad straight lines passed via origin with a correlation coefficient (R^2) 0.9598 were obtained (Fig. 11), that disavows the IPD model's applicability to all the data obtained from experiments for M.B dye. The values of q_t and K_{id} and C were found through curves of q_t versus $time^{1/2}$, and then data were listed in Table 2 [30, 31].

The liquid film diffusion (LFD) model could be established mechanistically as the following [32]:

$$\ln(1-F) = -k_{fd} \; x \; t \quad (4)$$

As the film diffusion coefficient is denoted by k_{fd} (min^{-1}) and F represents the fraction achievement of equilibrium ($F = q_t/q_e$). Plotting the liner plot result between ln (1−F) with time (t) and zero intercept, as exposed in Fig. 12, indicates that the diffusion of both CV and MB dyes via the liquid film surrounding the HCNC solid phase governed the adsorption process's.

3.4. Kinetic Models Study

The rate at which solid-phase sorbents remove dyes from aquatic solutions is important because it illustrates the mechanisms and chemical pathways of the adsorption process. Kinetic simulations for the extraction of CV as well as MB dyes via HSNC were computed using data from laboratory work regarding the effect of contact time [33]. The following formula can be used to express the kinetic model of the fractional power function (FPF) [34]:

$$\ln q_t = \ln \boldsymbol{a} + \boldsymbol{b} \ln t \quad (5)$$

where ***a*** and ***b*** are factors with b < 1, while qt (mg/g) is the amount of dyes adsorbed per gram of the HNNC solid-phase at any given time t. The adsorption process's data from experiments

is applied to the equation of the FPF**,** as seen in Fig. 13. The data come together well with the value of coefficient of the correlation (R^2) of 0.997 for CV dye and 0.995 for MB dye, as demonstrated in Table 2. This data may indicate that the kinetic model FPF is appropriate for explaining the adsorption of CV and MB dyes by HSNC solid phases.

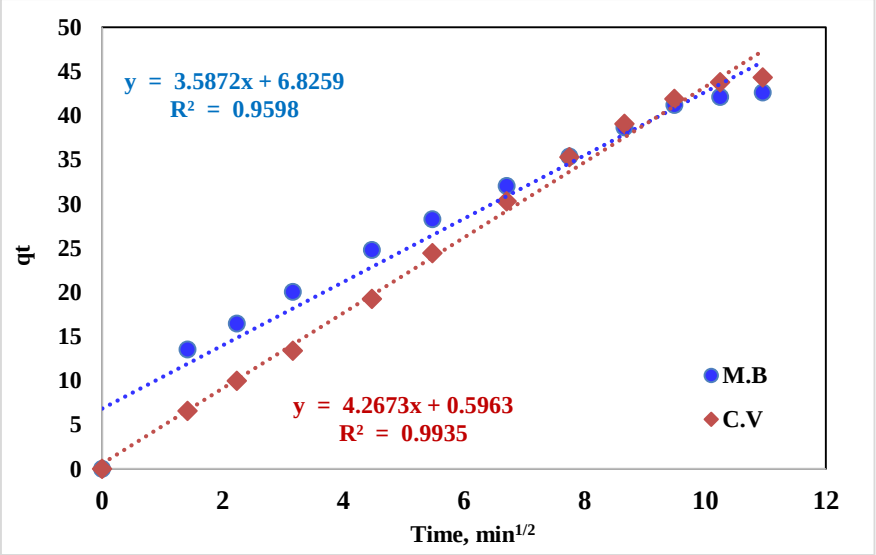

Fig. 11. Curve of Weber-Morris intraparticle diffusion model for adsorbed dyes (CV and MB) onto HSNC vs. time squared. The conditions of the experimental method were mentioned in Section 2.3.

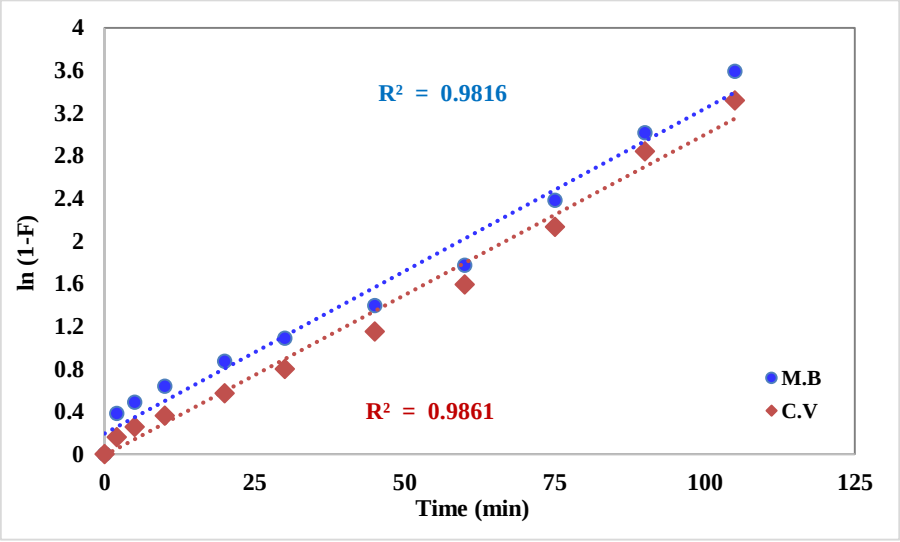

Fig. 12. Plot of liquid film diffusion (LFD) model for adsorbed dyes (CV and MB) onto HSNC.

The most popular formulas for describing adsorption rates in liquid-phase methods is the Lagergren equation or pseudo first order (PFO). The next equation was employed [34]:

$$\log\ (q_e - q_t) = \log q_e - \frac{K_{lag}}{2.303}\ t \qquad (6)$$

In which q_e and q_t are the quantities of adsorbed dyes (CV and MB) for every gram of HSNC at equilibrium and at any time t, in addition to K_{Lag} being the PFO rate constant. log (q_e - q_t) in

contradiction of the (t) plot (Fig. 14) was assigned a linear correlation. Determined K_{Lag}, q_e, and R^2 values intended for the removal of CV and MB dyes on HSNC solid phase are listed in Table 2. The PFO kinetics model for the adsorption of Crystal Violet dye onto HSNC solid phase is not supported by these results [35].

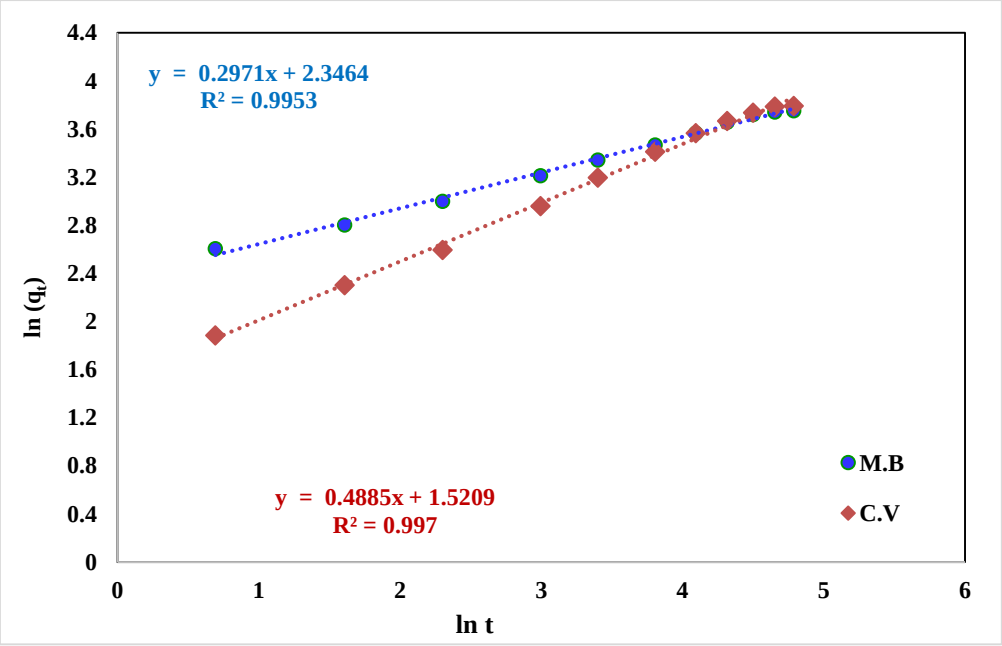

Fig. 13. Fractional power model curve for adsorbed dyes (CV and MB) onto HSNC. The conditions of the experimental method were mentioned in Section 2.3.

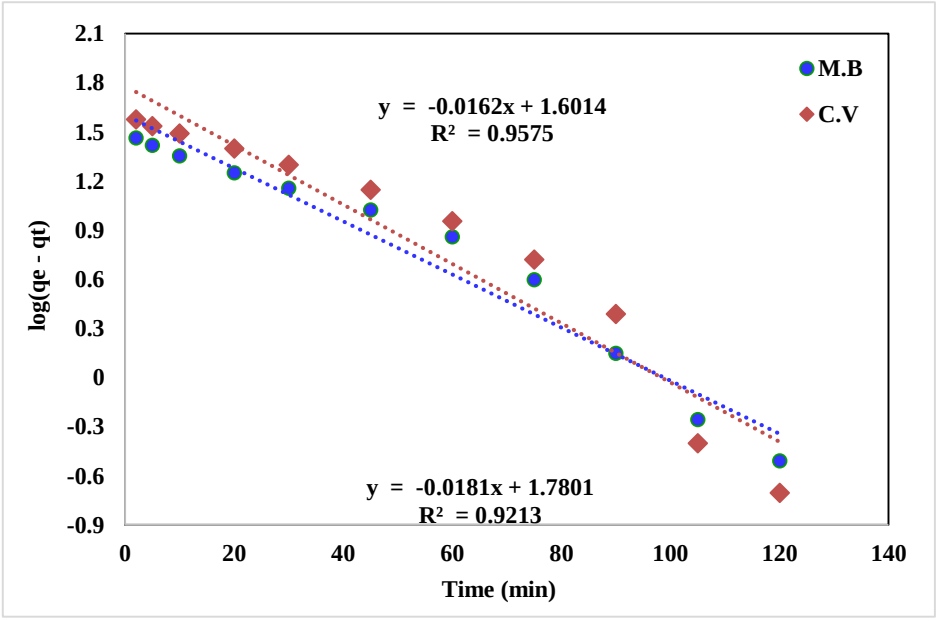

Fig. 14. Lagergren PFO curve for adsorbed dyes (CV and MB) onto HSNC. The conditions of the experimental method were mentioned in Section 2.3.

In contrast to the other models, the behavior is predicted across the whole adsorption range through pseudo-second-order (PSO) kinetic model, wherein chemisorption becomes rate-limiting step. The following equation represents PSO kinetic formula [36]:

$$\frac{t}{qt} = \frac{1}{k_2 q_e^2} + \left(\frac{1}{q_e}\right) t \tag{7}$$

In which q_t is the amount of dye that is adsorbed for grams of the HSNC solid state at any given time t, and q_e is amount of dyes that is removed from CV or MB per grams of HSNC at balance. The value of the coefficient of pseudo-second order is denoted by k_2. In these circumstances, the t/q_t versus t curves remained linear, as shown in Fig. 15. The uptake capacity (qe) at balance for dyes compounds and the coefficient of PSO (k_2) for C.V. and M.B. dyes were determined using the slope and intercept of the curves, and the data obtained are listed in Table 2. The results demonstrate that the kinetic PSO model's suitable for characterizing the adsorption technique of eliminating dyes by HSNC solid phase, and k_2, is often influenced by experimental parameter such as concentration, temperature, shaking time, and solution pH [37].

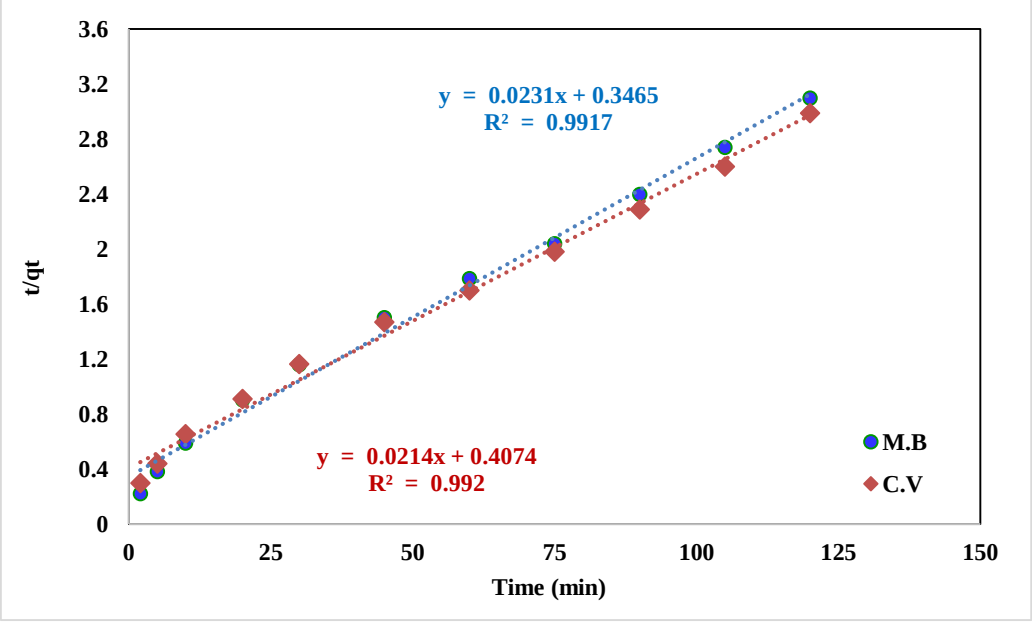

Fig. 15. Plots of the PSO for adsorbed dyes (CV and MB) onto HSNC. The conditions of the experimental method were mentioned in Section 2.3.

The rate equation is frequently described using the Elovich model, mostly based on their absorption capacity [38]. This model is particularly effective for determining chemisorption kinetics and is generally for instances when the absorbing external layer is not uniform. The next equation provides the model's interpretation:

$$q_t = \beta \ln(\alpha\beta) + \beta \ln t \tag{8}$$

In this case, the initial rate of adsorption (α) and its desorption coefficient (β) are the appropriate values. The Elovich model's α and β coefficients were found to have numerical values, and the graphs of q_t against ln t were linear, and from slope besides intercept of the curves of removal

CV and MB dyes onto HSNC as presented in (Fig. 16), the results data obtained were listed in Table 2.

The suitability of the PSO model was studied by performing the Chi-square test [36, 54]:

$$X^2 = \sum \frac{(q_{e,calc} - q_{e,exp})^2}{q_{e,calc}} \quad (9)$$

where $q_{e,exp}$ and $q_{e,calc}$ are the calculated and experimental amounts of CV and MB dyes adsorbed per unit mass of HSNC at equilibrium, respectively. The X^2 values for the PFO and PSO kinetic models for CV dye were equal to 4.21 and 0.13, respectively, and for MB dye, they were equal to 5.17 and 0.36, respectively. This data confirms the suitableness of PSO for the description of the adsorption process of CV and MB dyes on the HSNC solid phase.

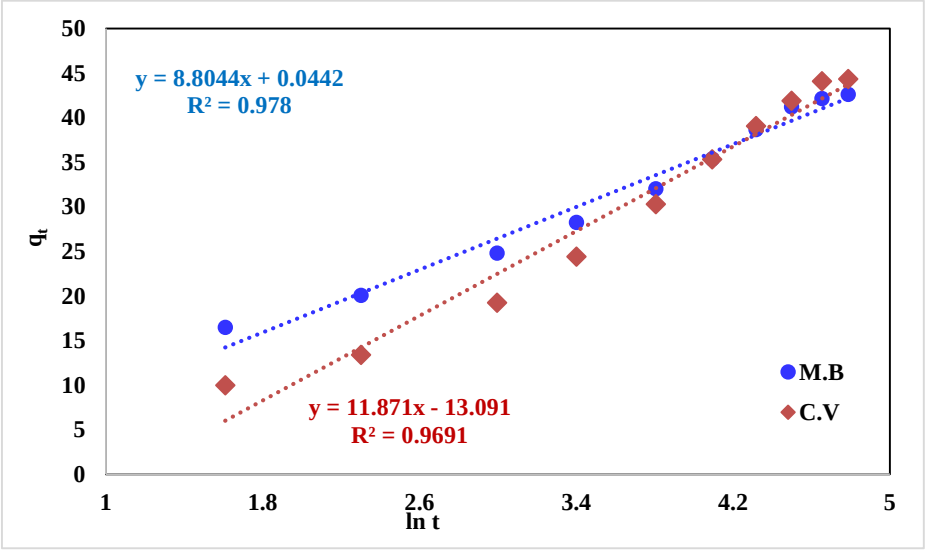

Fig. 16. Curves of the Elovich model for adsorbed dyes (CV and MB) onto HSNC. The conditions of the experimental method were mentioned in Section 2.3.

Based on the above results and correlation coefficient values and comparison between the close values of q_e examination with q_e calculated (listed in Table 2) and the Chi-square test, the elimination of CV and MB dyes by HSNC occurs through a variety of mechanisms, such as IPD and LFD, but these processes do not determine the rate of elimination. Additionally, it is demonstrated that the PSO kinetic model is the most applicable kinetic model to define the adsorption process of CV and MB dyes on the HSNC solid phase [39].

3.5 Adsorption Isotherms of CV and MB Dyes on HSNC Solid Phase

The process of interaction between the dyes (CV and MB) on the HSNC sorbent layer was explained using adsorption isotherms. The equilibrium investigations are helpful in determining several significant surface features of the investigated sorbent as well as the maximum adsorption capacity of HSNC towards CV as well as MB dyes, according to the kind of adsorption mechanism. Critical analysis was done on the retention patterns throughout a range of equilibrium values (1–12.5 mg/L) via the aquatic solutions containing dyes on the utilized sorbent under ideal conditions. Figure 17 shows the quantity of dyes maintained on the HSNC against the equilibrium levels of dyes (CV and MB) in solution. The quantity of dyes

that were maintained in the solution correlated linearly with the quantity of dyes kept on the HSNC at moderate sample concentrations. The uptake capacity for CV was found to be 43.97 ± 0.12 mg/g, and for MB was found to be 42.63± 0.11 mg/g of dyes onto the HSNC solid phase.

Table 2. Various diffusion and kinetic model parameter for dyes (CV and MB) adsorption onto HSNC at 295 K.

Intraparticle diffusion (IPD)				
	K_{id} (mg/g $min^{1/2}$)	C (mg/g)		R^2
CV	4.267	0.596		0.993
MB	3.587	6.826		0.959
Liquid film diffusion (LFD)				
	K_{fd} (min^{-1})			R^2
CV	0.030			0.986
MB	0.031			0.982
Fractional power function (FPF)				
	a		b	R^2
CV	4.577		0.488	0.997
MB	10.44		0.297	0.995
Lagergren (PFO)				
	$q_{e,\,exp}$	$q_{e,\,calc}$	k_1	R^2
CV	44.32 mg/g	60.25 mg/g	0.042	0.971
MB	42.6 mg/g	39.81 mg/g	0.038	0.957
Pseudo second order (PSO)				
	$q_{e,\,exp}$ (mg/g)	$q_{e,\,calc}$ (mg/g)	k_2	R^2
CV	44.32	46.72	1.1 x 10^{-3}	0.992
MB	42.6	43.47	1.5 x 10^{-3}	0.992
Elovich kinetic				
	α (g/mg min)	β (mg/g min)		R^2
CV	0.028	11.78		0.964
MB	0.114	8.804		0.978

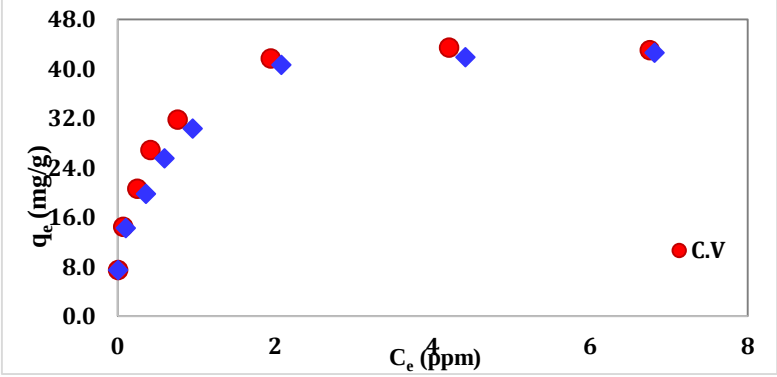

Fig. 17. Plot of CV and MB dyes retained (q_e) onto the HSNC solid phase (mg/g) against equilibrium concentration (C_e), at 22 ºC.

The next form of linearity represents the Langmuir isotherm equation applied to the retention of CV and MB dyes on HSNC sorbent [40]:

$$\frac{C_e}{q_e} = \frac{1}{q_m k_L} + \frac{C_e}{q_m} \qquad (10)$$

In which C_e represents the equilibrium conc. (mg/L) of dyes (CV and MB) in the test solution and q_e is the quantity of dyes adsorbed for each unit mass of adsorbent after equilibrium (mg/g). The constants q_m and K_L characterize the Langmuir parameter, which is related to the greatest

solute capacity for adsorption per unit mass of adsorbent needed for monolayer surface protection, and the equilibrium constant, which is associated with the temperature-independent binding energy of solute adsorption, individually. The chart of C_e/q_e vs. C_e during all the concentration varieties of CV and MB dyes onto HSNC was linear (Fig. 18), with (R^2) equal 0.9985 for CV dye and 0.9947 for MB dye, indicating that the removal of the CV and MB dyes on HSNC adsorbent is homogeneous and fits well with Langmuir. The quantities of q_m and K_L derived from the linear plot's slope and intercept are listed in Table 3. The fundamental feature of this model is the dimensionless separation factor, R_L, which is described as:

$$R_L = \frac{1}{1+ K_L C_o} \tag{11}$$

R_L values for the adsorbent equal 0.396 for CV and 0.424 for MB dyes ($0 < R_L < 1$), which indicates favorable monolayer adsorption [41].

The retention behavior of CV and MB dyes from aquatic solutions onto the used sorbents was subjected to the Freundlich system, which represents the next form of linearity [42]:

$$\log q_e = \log K_F + (1/n) \log C_e \tag{12}$$

K_F and 1/n are Freundlich parameters associated with the maximal solute adsorption capacity (mg/g), q_e is the concentration of the retained CV and MB dyes on the HSNC per unit mass (mg/g) at equilibrium, and C_e is the conc. of CV and MB dyes remained in the aqueous solution (mg/L). Table 3 lists the estimated values of the Freundlich parameters K_F and 1/n that were calculated using the intercept and slope (see Fig. 19). The 1/n value was found to be equal to 0.266 for CV and 0.272 for MB dyes, which is a lesser amount than unity ($1/n < 1$), thus sorbents' surfaces were favorable for the adsorption of CV and MB dyes by the HSNC. The correlation coefficients (R^2) of Freundlich model for CV and MB dyes do not have good values (as seen in Table 3), which recommends that the adsorption model is better explained by the Langmuir model. This result is consistent with what has been published about the extraction of CV and MB using different sorbents [27, 42, 43] for CV and [27, 44, 45] for MB.

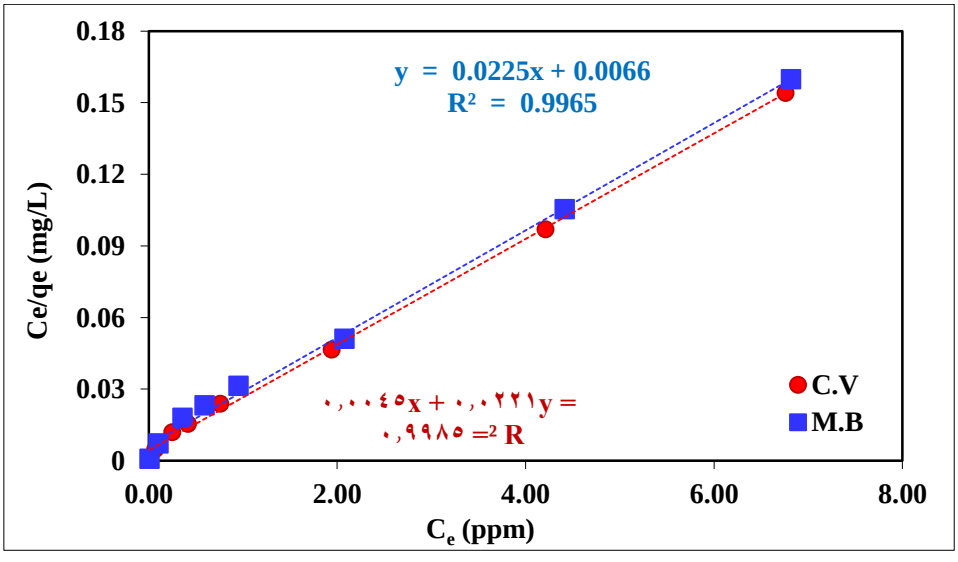

Fig. 18. Langmuir isotherms for adsorption of CV and MB dyes on the HSNC at 22 oC.

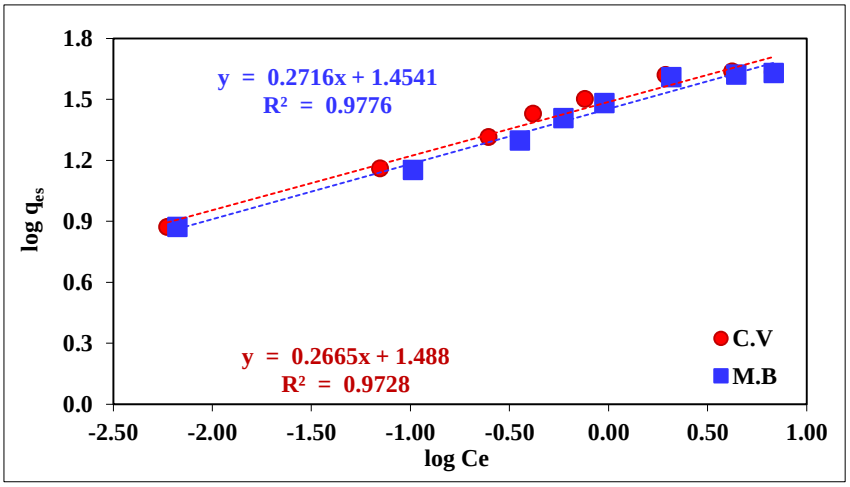

Fig. 19. Plot of log C_{ads} vs log C_e of CV and MB dyes retention onto HSNC at 22 ºC. (Freundlich isotherms).

Table 3. The parameter of isotherm models for the retention of CV and MB dyes on HSNC solid phase at 22 ˚C.

Models of adsorption isotherms		CV dye	MB dye
Langmuir	q_m,	45.25 mg/g	44.44 mg/g
	K_L,	0.204 L/g	0.182 L/g
	R_L	0.396	0.424
	R^2	0.9985	0.9947
Freundlich	K_F,	30.76 mg/g	28.44 mg/g
	1/n	0.266	0.272
	R^2	0.973	0.977

3.6. Thermodynamic Studies

Thermodynamic characteristics Investigations aimed at the adsorption of CV and MB dyes on HSNC at a broad variety of temperatures (283-323 K) were studied. The following formula was used to compute the thermodynamic parameters, containing enthalpy (ΔH), Gibbs free energy (ΔG), and entropy (ΔS) [22]:

$$\ln K_c = \frac{-\Delta H}{RT} + \frac{\Delta S}{R} \tag{13}$$

$$\Delta G = \Delta H - T\Delta S \tag{14}$$

$$\Delta G = RT \ln K_c \tag{15}$$

In which R is the constant of the gas, KC is the constant of the equilibrium, and T is the temperature expressed in Kelvin. Values calculation of constant K_C for the removal of CV and MB dyes by the next equation:

$$\boldsymbol{k_c = \frac{C_a}{C_e}} \tag{16}$$

The concentration of CV and MB dyes in aquatic solution at equilibrium is represented by C_e (mg/L), whereas C_a (mg/L) characterizes the concentration of dyes absorbed on the solid surface for each milliliter at equilibrium. The curve of ln K_C vs. 1000/T for dyes adsorption onto HSNC was linear (Fig. 20) within a temperature range of 283–323 K. As the temperature

rises, the equilibrium constant of CV and MB dyes increases, and the endothermic behavior of the dyes adsorption on HSNC is indicated by the positive value of enthalpy (ΔH). As shown in Fig. 20, the values of (ΔH), (ΔS), and (ΔG) at 295 K were calculated using the straight line of ln K_C vs. 1000/T. The heats of activation ΔH, which correspond to CV and MB, were determined to be 51.38 ± 1.89 and 35.14 ± 1.23 kJ/mol, respectively. The corresponding activation entropies, ΔS, were determined as 186.9 ± 3.26 and 128.8 ± 2.98 J/K mol for CV and MB, respectively. The free energy, ΔG, was calculated using Eq. (13) as -3.75 ± 0.11 and -2.85 ± 0.09 kJmol^{-1} for CV and MB, respectively. A positive value of ΔS for CV and MB dyes recommends an increase in the degree of flexibility on the solid-liquid connection, which indicates the binding of CV and MB dyes species. The negative values of (ΔG) at 295 for CV and MB dyes suggest the dyes' spontaneous adsorption properties on the HSNC solid phase. Also, the values of (ΔH) indicate that the removal of dyes onto HSNC was due to the chemical nature of the adsorption process for CV dye and the physical nature of the adsorption process for MB dye.

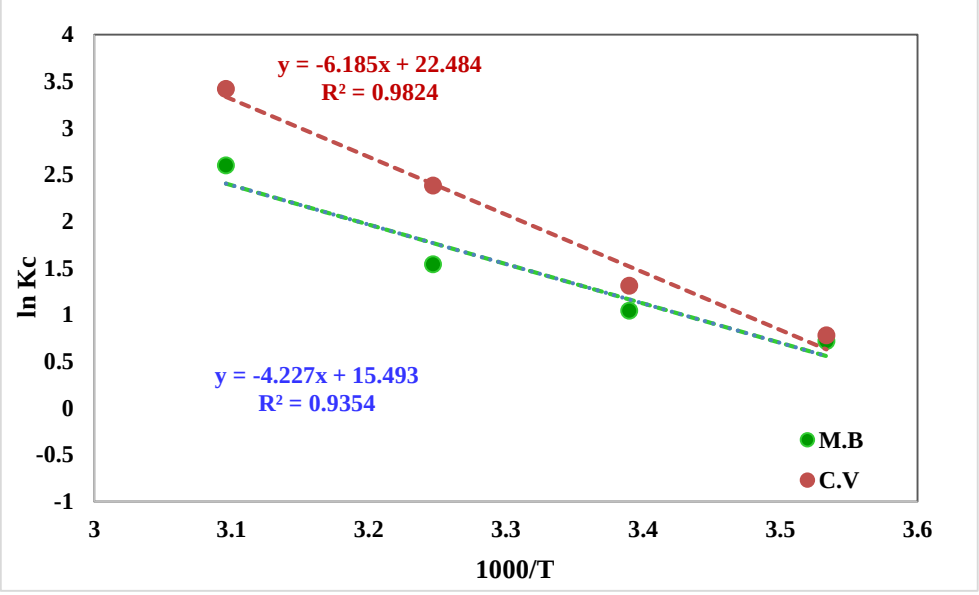

Fig. 20. Influence of ln K_c vs 1000/T for CV and MB dye adsorption on HSNC.

3.7. Applications Study

The efficiency of this method was confirmed by testing real samples of the surroundings. Samples of tap water, wastewater, and seawater were collected and processed in accordance with Section 2.6. After analysis, the amount of CV and MB dyes in all samples was discovered to be less than the limit of detection of UV–vis. The samples were then spiked with CV and MB dyes (7.5 mg/L) and shaken for 120 minutes with 25 mg of HSNC after the pH was adapted to 9 and 8 for CV and MB dyes, respectively, at 295 K. The removal percentages of CV and MB dyes in the actual samples; wastewater, seawater, and tap water were determined to be 96.7%, 95.3%, and 97.9% for CV dye also were discovered 92.8%, 94.4%, and 97,1% for MB dye.

After the removal method, the HSNC solid phase were collected and washed several times with acetone to remove the dyes, then dried to test their reusability. The reusability of HSNC

for the removal of CV and MB from the aqueous solution was investigated. The outcomes demonstrated that, under the optimum conditions, HSNC could be applied four times in a row to effectively remove MB and CV from the aqueous solution while maintaining the highest removal percentage. Finally, the comparison of this method and the previous literature for adsorption CV and MB is listed in Table 4. The table indicates evidence that HSNC may be regarded as an effective and attractive solid phase for adsorbing CV and MB dyes from aquatic environments.

Table 4. Comparing the HSNC with previous adsorbents in order to remove CV and MB dyes

dye	Solid phase adsorbents	q_e (mg/g)	Reference
CV	Agricultural waste residue	12.2	[46] 2020
CV	Lemonwood activated carbon	23.6	[47] 2021
CV	Treated sugarcane bagasse	59.3	[27] 2022
CV	Charred rice husk	62.85	[48] 2022
CV	Composite material from rice husk ash	11.06	[42] 2023
CV	Fucus spiralis biomaterial	53	[49] 2024
CV	Ulva intestinalis biomaterial	55	[49] 2024
CV	**Halloysite nanoclay**	**46.72**	**This work**
MB	Green tea dredge	71.4	[45] 2013
MB	Sugarcane bagasse	12.42	[50] 2020
MB	Treated sugarcane bagasse	58.9	[27] 2022
MB	sodium alginate hydrogel	51.34	[51] 2023
MB	Magnetic chitosan-PEGDE-EDTA composite	5.04	[52] 2023
MB	Activated Corn husk waste	41.06	[53] 2024
MB	**Halloysite nanoclay**	**43.47**	**This work**

4. Conclusions

The current study showed that the solid Halloysite nanoclay can be used for removing Methylene Blue and Crystal Violet dyes. The physical characterization of the HSNC was studied using SEM, FTIR, TEM, BET, and XRD. The analysis data showed a hollow tubular structure in HSNC with about 1 μm length, 60 nm diameter, and a 72.8 m^2/g specific surface. The best conditions of mass, pH solution, shaking period, temperature, and, in addition, KNO_3 concentration, on the removal/adsorption efficacy of CV and MB dyes by HSNC were studied. The second-order kinetic system was found to be the finest model to describe the adsorption process through uptake capacity ($q_{e,cal}$) values of 46.72 mg/g for CV and 43.47 mg/g for MB dyes on HSNC. The removal of the CV and MB dyes by HSNC solid phase is homogeneous and fits well with the Langmuir model of isotherm. The thermodynamic analysis of the adsorption of CV and MB dyes was endothermic, which suggests the dyes' physical and spontaneous adsorption properties on the HSNC solid phase. Finally, the HSNC solid phase was successful in removing dyes in three real samples (sea water, wastewater, and tap water) with a great percentage of 92.7 - 97.8%.

References

[1] R. A. Mansour, M. G. Simeda, A. A. Zaatout, RSC Adv.,11 (2021) 7851. https://doi.org/10.1039/D0RA08488C

[2] M. Neamtu, I. Siminiceanu, A. Yediler, A. Kettrup, Dyes Pigments. 53 (2002) 93-99. https://doi.org/10.1016/S0143-7208(02)00012-8

[3] R. Foroutan, R. Mohammadi, N Sohrabi, S Sahebi, S. Farjadfard, Z. Esvandi, B. Ramavandi, Environ Technol Innovat 17 (2020) 100530. https://doi.org/10.1016/j.eti.2019.100530

[4] Grassi P, Drumm FC, Spannemberg SS, Georgin J, Tonato D, Mazutti MA, et al., Environ Sci Pollut Res 27 (2020)10484-1094. https://doi.org/10.1007/s11356-020-07664-0

[6] S. Sonal, B. K. Mishra, Water Pollut. Manage. Pract., (2021) 303-331, http://dx.doi.org/10.1007/978-981-15-8358-2_13

[7] E. Al-Abbad, F. Alakhras, Indones. J. of Sci. & Technol., 5 (2020) 352-365, https://doi.org/10.17509/ijost.v5i3.24986

[8] L. Nahali, Y. Miyah, F. Mejba, M. Benjelloun, O. Assila, Y. Fahoul, V. Nenov, F. Zerrouq, Desalin. Water Treat., 245 (2022) 255–269, http://dx.doi.org/10.5004/dwt.2022.27945

[9] C. Rekhate, J.K. Shrivastava, Sci. Eng., 42 (2020) 492-506, https://doi.org/10.1080/01919512.2020.1714426

[10] C. Osagie, A. Othmani, S. Ghosh, A. Malloum, Z. Esfahani, S. Ahmadi, J. Mater. Res. Technol. 14 (2019) 2195-2218, https://doi.org/10.1016/j.jmrt.2021.07.085

[11] I. Anastopoulos, I. Pashalidis, A. G. Orfanos, I. D. Manariotis, T. Tatarchuk, L. Sellaoui, A. Bonilla-Petriciolet, A. Mittal, A. Núñez-Delgado, J. Environ. Manage., 261 (2020) 110236, https://doi.org/10.1016/j.jenvman.2020.110236

[12] A. Mohammadi, P. Veisi, J. Environ. Chem. Eng. 6 (2018) 4634-4643, https://doi.org/10.1016/j.jece.2018.07.002

[13] N. Aljohani, R. K. Al-Farawati, I. I. Shabbaj, B. A. Al-Mur Y.N Kavil, M. Abdel Salam, Water 13 (2021) 969, https://doi.org/10.3390/w13070969

[14] H. A. Ewais, Russian J. Phys. Chem. A, 96 (2022) 119–127, https://doi.org/10.1134/s0036024422140096

[15] A.N. Tchakounte, B.A. Ateba, Ngop Pulcherie, D.J. Dina, J.M. Dika, C.M. Kede, J. Appl. Surf. Interfaces 9 (2021) 1–13, https://doi.org/10.48442/IMIST.PRSM/jasi-v9i1-3.26041

[16] H. A. Ewais, A. S. Basaleh, Y. M. Al Angari, Int. J. Chem. Kinet., 55 (2023) 271–280.

https://doi.org/10.1002/kin.21634

[17] M. Abdel-Salam, L.A. Al-khateeb, M.A. Abdel-Fadeel, Desal. Water Treat., 129 (2018) 168–176, http://dx.doi.org/10.5004/dwt.2018.23085

[18] Md. I. Hossain., M. M. Soliman, M. El-Naggar, Md. Z. Sultan, A. Kechi, N. R. Abdelsalam, M.A. Abu-Saied, M. Chowdhury, J. Mater. Res. Technol. 12 (2021) 1715-1727, https://doi.org/10.1016/j.jmrt.2021.03.097

[19] D. A. Almasri, T. Rhadfi, M. A. Atieh, G. McKay, S. Ahzi, Chem Eng J, 335 (2018) 1-12, https://doi.org/10.1016/j.cej.2017.10.031

[20] I. Anastopoulos, A. Mittal, M. Usman, J. Mittal, G. Yu, A. Núñez-Delgado, M. Kornaros, J. Mol. Liq. 269, (2018) 855–868, https://doi.org/10.1016/j.molliq.2018.08.104

[21] R. G. Kaling T. M. Kumar, Environ. Nanotechnol. Monit. Manage 20 (2020) 100339. https://doi.org/10.1016/j.enmm.2020.100339

[22] D. F. Katowah. M. A. Abdel-Fadeel, Nanocomposites, 9 (2023) 80–99. https://doi.org/10.1080/20550324.2023.2251677

[23] Z. Marczenko, 2nd ed., John Wiley and Sons, 1986, https://www.osti.gov/biblio/6723640-separation-spectrophotometric-determination-elements

[24] B. Koh, W. Cheng, Langmuir, 30 (2014) 10899–10909, https://doi.org/10.1021/la5014279

[25] H. Senoussi, H. Osmani, C. Courtois, M. Bourahli, el H., Boletín La Soc. Española Cerámica Y Vidr. 55 (2016)121–126, https://doi.org/10.1016/j.bsecv.2015.12.001

[26] S. Ramanayaka, B. Sarkar, A. T. Cooray, Y. S. Ok, M. Vithanage, J. Hazard Mater 384 (2020) 121301, https://doi.org/10.1016/j.jhazmat.2019.121301

[27] A. S. Omer, G. A.El Naeem, A.I. Abd-Elhamid, O. O.M. Farahat, A. A. El-Bardan, H. M.A. Soliman, A.A. Nayl, J Mater Res Technol., 19 (2022) 3241-3254, https://doi.org/10.1016/j.jmrt.2022.06.045

[28] S.A. Dastgheib, D.A. Rockstraw, Carbon 40 (2002) 1853–1861, https://doi.org/10.1016/S0008-6223(02)00036-2

[29] W.J. Weber, J.C. Morris, J. Sanit, Eng. Div. Am. Soc. Civ. Eng. 89 (1963) 31–36, https://doi.org/10.1061/JSEDAI.0000430

[30] A.K. Bhattacharya, C. Venkobachar, J. Environ. Eng. 110 (1984) 1–299, https://doi.org/10.1061/(ASCE)0733-9372(1984)110:1(110)

[31] R. H. Althomalia, K. A. Alamrya, M. A. Husseina, A. Khana, S. S. Al-Juaida and A. M. Asiri, Int. J. Environ. Anal. Chem., 12 (2020) 1-12. https://doi.org/10.1080/03067319.2020.1772772

[32] G. E. Boyd, A. W. Adamson, L. S. Myers, J. Am. Chem. Soc. 69 (1947) 2836–2848. https://doi.org/10.1021/ja01203a064

[33] S. Palagyi, T. Braun, CRC Press, Boca Raton, FL, 1992, https://www.osti.gov/biblio/5468657-preconcentration-techniques-trace-elements

[34] H. M. Al-Saidi, M. A. Abdel-Fadeel, S. S. Alharthi, J. Saudi Chem. Soc, 25 (2021) 101301. https://doi.org/10.1016/j.jscs.2021.101301

[35] M.A. Gabal, N.G. Al-Zahrani, Y.M. Al Angari, M.A. Abdel-Fadeel, S.R. Alharbi, R.M. El-Shishtawy Mater. Res. Express. 6 (2019) 105059. https://doi.org/10.1088/2053-1591/ab3b88

[36] S. A. Hameed, M. A. Abdel-Fadeel, H. M. Al-Saidi, M. Abdel Salama Water Treat., 188 (2020) 266-276. http://dx.doi.org/10.5004/dwt.2020.25348

[37] T. Braun, J.D. Navratil, A.B. Farag, Polyurethane Foam Sorbents in Separation Science, CRC Press Inc., Boca Raton, FL, 1985. https://doi.org/10.1201/9781351075916

[38] M. A. Abdel-Fadeel, N. S. Aljohani, S. R. Al-Mhyawi, R. F. Halawani, E. H. Aljuhani, M. Abdel Salam, J. Saudi Chem. Soc. 26 (2022) 101475. https://doi.org/10.1016/j.jscs.2022.101475

[39] N. Rahman, P. Varshney, M. Nasir, Environ. Nanotechnol. Monit. Manage., 15 (2021)100458. https://doi.org/10.1016/j.enmm.2021.100458

[40] I. Langmuir, J. Am. Chem. 57 (1918) 1361–1403, https://doi.org/10.1021/ja02242a004

[41] O. Sacco, M. Matarangolo, V. Vaiano, G. Libralato, M. Guida, G. Lofrano, M. Carotenuto, Sci. Total Environ. 644 (2018) 430–438, https://doi.org/10.1016/j.scitotenv.2018.06.388

[42] A. S. Sidjou, A. N. Tchakounte, V. Shikuku, I. Lenou, R. Djimtibaye, M. M. Dika, Hybrid Advances, 4 (2023) 100113. https://doi.org/10.1016/j.hybadv.2023.100113

[43] N. Howell, A. Pimentel, S. Bhattacharia, Environ. Challenges, 4 (2021) 100137, https://doi.org/10.1016/j.envc.2021.100137

[44] R.R. Krishni, K.Y. Foo, B.H. Hameed, Desal. Water Treat 52 (2014) 6104–6112. https://doi.org/10.1080/19443994.2013.815687

[45] M. Ahmad, R. T. Bachmanna, M. Ain Khan, R. G.J. Edyvean, U. Farooq, M. M. Athar, Desal. Water Treat. 50 (2013) 1–10, http://dx.doi.org/10.1080/19443994.2013.867818

[46] I. Loulidi, F. Boukhlifi, M. Ouchabi, A. Amar, M. Jabri, A. Kali, S. Chraibi, C. Hadey, F. Aziz, , Sci. World J. (2020) 5873521, https://doi.org/10.1155/2020/5873521

[47] R. Foroutan, S.J. Peighambardoust, S.H. Peighambardoust, M. Pateiro, J. M. Lorenzo, Molecules 26 (8) (2021) 2241. https://doi.org/10.3390/molecules26082241

[48] P.L. Homagai, R. Poudel, S. Poudel, A. Bhattarai, Heliyon 8 (4) (2022), e09261, https://doi.org/10.1016/j.heliyon.2022.e09261

[49] L. Boukarma, R. Aziam, A. Aboussabek, S. El Qdhy, M. Zerbet, F. Sinan, M. Chiban, Bioresource Technology, 394 (2024) 130197, https://doi.org/10.1016/j.biortech.2023.130197

[50] N.T.H Anh, T. T. Phuc, T. N. M. An, P. Q. Hue, N. V. Cuong, Indones. J. Chem. 20 (2020) 1101–1109, http://dx.doi.org/10.22146/ijc.48713

[51] A. Allangawi, M. A. Aziz Aljar, K. Ayub, A.Abd El-Fattah, J. Mol. Graph. Model., 122 (2023) 108468. https://doi.org/10.1016/j.jmgm.2023.108468

[52] R. Rahmi, L. Lelifajri, F. Fathurrahmi, H. Fathana, M. Iqhrammullah, S. Afr. J. Chem. Eng., 43 (2023) 296–302, https://doi.org/10.1016/j.sajce.2022.11.009

[53] T. Handayani, Emriadi, Deswati, P. Ramadhani, R. Zein, S. Afr. J. Chem. Eng., 47 (2024) 15–27. https://doi.org/10.1016/j.sajce.2023.10.003

[54] V. Bagdonavicius, M.S. Nikulin, Chi-square goodness-of-fit test for right censored data, Int. J. Appl. Math. Stat., 24 (2011) 30–50. https://www.researchgate.net/publication/325193712

مبسط لمعالجة صبغتي الميثيلين الأزرق والكريستال البنفسجي من المحلول المائي باستخدام مادة الطين النانونية: دراسات حركية، وتوازن، وديناميكا حرارية

محمد عبد الفاضل

قسم الكيمياء، كلية العلوم، جامعة الملك عبد العزيز، جدة ٢١٥٨٩، المملكة العربية السعودية، والمختبر الطبي الحيوي، مستشفى الصدر، المنصورة، الدقهلية، مصر

m_abdelazeem@hotmail.com

المستخلص. يوضح هذا البحث طريقة سريعة وبسيطة وسهلة وصديقة للبيئة لإزالة صبغتي الكريستال البنفسجي (CV) والأزرق الميثيليني (MB) من المحلول المائي بواسطة سطح صلب صديق للبيئة مكون من طين الهالوسيت النانوني (HSNC). تمت دراسة الخصائص الفيزيائية لـ HSNC باستخدام تقنيات مثل SEM وTEM وXRD وFTIR وBET. وقد تم فحص عدة عوامل تؤثر على كفاءة الامتزاز، بما في ذلك درجة الحموضة (pH) للمحلول، وكمية المادة الماصة، ودرجة الحرارة، ووقت الاهتزاز، وتركيز (KNO_3) نترات البوتاسيوم. كذلك تمت دراسة كفاءة امتزاز صبغتي CV وMB على HSNC باستخدام حسابات الطرق الحركية، وأظهرت البيانات أن عمليات الامتزاز تحدث عبر نظام من الرتبة الثانية الوهمية (PSO)، حيث بلغت السعة المحسوبة لقيم الامتزاز ٤٦,٧٢ ($q_{e,cal}$) ملجم/جم لصبغة CV و٤٣,٤٦ ملجم/جم لصبغة MB على سطح المدة المازة. كذلك وجد أن نموذج لانجمير هو الأنسب لشرح سلوك التوازن لإزالة الصبغات على HSNC تحت أفضل الظروف، مع سعة امتزاز قصوى (q_m) بلغت ٤٥,٢٥ ملجم/جم لصبغة CV و٤٤,٤٤ ملجم/جم لصبغة MB. كما تشير الدراسة الديناميكية الحرارية إلى أن إزالة صبغتي CV وMB هي عملية ماصة للحرارة، وأن الامتزاز يتم بطريقة كيميائية وتلقائية. أخيرًا، أعطت اختبارات كفاءة إزالة صبغتي CV وMB بناءً على ثلاثة عينات فعلية مختلفة على سطح المادة المازة HSNC نسبة كفاءة (E%) تزيد عن ٩٣%. وبشكل عام، اكتُشف أن HSNC مادة منخفضة التكلفة وصديقة للبيئة لإزالة صبغات CV وMB الكاتيونية.

الكلمات المفتاحية: الكريستال البنفسجي، الميثيلين الأزرق، النانو كلاي، الإزالة، الحركية، الإيزوثيرم، الديناميكا الحرارية.